

# RSC Advances



This is an *Accepted Manuscript*, which has been through the Royal Society of Chemistry peer review process and has been accepted for publication.

*Accepted Manuscripts* are published online shortly after acceptance, before technical editing, formatting and proof reading. Using this free service, authors can make their results available to the community, in citable form, before we publish the edited article. This *Accepted Manuscript* will be replaced by the edited, formatted and paginated article as soon as this is available.

You can find more information about *Accepted Manuscripts* in the [Information for Authors](#).

Please note that technical editing may introduce minor changes to the text and/or graphics, which may alter content. The journal's standard [Terms & Conditions](#) and the [Ethical guidelines](#) still apply. In no event shall the Royal Society of Chemistry be held responsible for any errors or omissions in this *Accepted Manuscript* or any consequences arising from the use of any information it contains.

## Synthesis and electrochemical performance of $\text{Li}_4\text{Ti}_5\text{O}_{12}/\text{TiO}_2/\text{C}$ nanocrystallines for high-rate lithium ion batteries

Wenjun Zhu <sup>a</sup>, Hui Yang <sup>a</sup>, Wenkui Zhang <sup>b</sup>, Hui Huang <sup>b</sup>, Xinyong Tao <sup>b</sup>, Yang Xia <sup>b</sup>,  
Yongping Gan <sup>b</sup> and Xingzhong Guo <sup>a\*</sup>

<sup>a</sup>*School of Materials Science and Engineering, Zhejiang University, 38 Zheda Road, Xihu District, Hangzhou 310027, China*

<sup>b</sup>*College of Materials Science and Engineering, Zhejiang University of Technology, Hangzhou 310014, China.*

$\text{Li}_4\text{Ti}_5\text{O}_{12}/\text{TiO}_2/\text{Carbon}$  ( $\text{Li}_4\text{Ti}_5\text{O}_{12}/\text{TiO}_2/\text{C}$ ) nanocrystalline composite has been successfully synthesized by a facile sol-gel method and subsequent calcination treatment, and pure  $\text{Li}_4\text{Ti}_5\text{O}_{12}$ ,  $\text{Li}_4\text{Ti}_5\text{O}_{12}/\text{C}$  and  $\text{Li}_4\text{Ti}_5\text{O}_{12}/\text{TiO}_2$  composites have also been synthesized in the present study for comparison. All the samples present a nanocrystalline structure with a uniform size distribution, and abundant phase interfaces can be detected for  $\text{Li}_4\text{Ti}_5\text{O}_{12}/\text{TiO}_2$  and  $\text{Li}_4\text{Ti}_5\text{O}_{12}/\text{TiO}_2/\text{C}$  composites. Electrochemical measurements demonstrate that the resultant  $\text{Li}_4\text{Ti}_5\text{O}_{12}/\text{TiO}_2/\text{C}$  composite exhibits a superior rate capability and cycle stability in comparison with pure  $\text{Li}_4\text{Ti}_5\text{O}_{12}$ ,  $\text{Li}_4\text{Ti}_5\text{O}_{12}/\text{C}$  and  $\text{Li}_4\text{Ti}_5\text{O}_{12}/\text{TiO}_2$  composites, which can be attributed to high grain boundary density, abundant phase interfaces and *in situ* formed carbon, for storing extra lithium ions, enhancing rapid lithium insertion/extraction kinetics and improving electron transport rate.

---

Corresponding author. Fax: +86 571 87953054. E-mail address: msewj01@zju.edu.cn (X. Z. Guo).

## Introduction

Rechargeable lithium-ion batteries (LIBs) have attracted great attention as the power source for most portable electronic devices and a promising energy-storage device in electric vehicle and electrical/hybrid vehicles, due to large energy density, environmental friendliness and high output voltage.<sup>1-6</sup> With the rapid development of portable electronic devices and hybrid electric vehicles, it is highly desired to explore new LIBs materials with high power density, long cycle life, and better safety. Currently, carbonaceous materials have been used as the most common commercial anode materials for LIBs. However, the carbonaceous materials have some safety concerns, particularly when used for high power batteries. Lithium dendrites are likely to be formed on the surface of carbon materials after long charge-discharge cycles, resulting in the capacity decay.<sup>7-9</sup> Therefore, searching for alternative anode materials with excellent rate-capability and good safety property becomes the urgent topic for the LIBs field.<sup>3, 10-13</sup>

Spinel lithium titanium oxide ( $\text{Li}_4\text{Ti}_5\text{O}_{12}$ ) has garnered particular interests as one of the most attractive LIBs anode materials owing to the stable and high flat Li ion insertion voltage ( $\sim 1.55$  V vs.  $\text{Li}/\text{Li}^+$ ), which could effectively avoid the formation of the solid-electrolyte interphase (SEI) layer and suppress the deposition of lithium dendrites, largely enhance the safety of the cells. Moreover, the negligible volume change of spinel  $\text{Li}_4\text{Ti}_5\text{O}_{12}$  electrode during the repeated  $\text{Li}^+$  insertion and extraction processes guarantees the long-term electrochemical stability and the enhanced capacity retention.<sup>14-16</sup> Thus, spinel  $\text{Li}_4\text{Ti}_5\text{O}_{12}$  is considered as a promising alternative

to carbonaceous anodes. Despite of these advantages, the practical application of spinel  $\text{Li}_4\text{Ti}_5\text{O}_{12}$  is still largely restrained by the inherently kinetic problem derived from the low electronic conductivity ( $10^{-13} \text{ S}^{-1}$ ) and sluggish lithium ion diffusion ( $10^{-13}$  to  $10^{-9} \text{ cm}^2 \text{ s}^{-1}$ ), resulting in a poor rate capability.<sup>8, 17-19</sup>

Up to date, tremendous efforts have been made to circumvent the drawbacks of  $\text{Li}_4\text{Ti}_5\text{O}_{12}$ . An effective strategy is reducing the particle size of  $\text{Li}_4\text{Ti}_5\text{O}_{12}$  to nanoscale range to acquire enhanced electrochemical performance by shortening the diffusion paths for electrons and lithium ions.<sup>15, 20, 21</sup> Another effective strategy is synthesizing nanocomposites coating with conductive carbonaceous materials, such as graphite, graphene, carbon nanotubes, and carbon nanofibers, etc., which could effectively increase the electrical conductivity to further enhance the electrochemical performance of  $\text{Li}_4\text{Ti}_5\text{O}_{12}$  electrode, especially the rate capability.<sup>2, 7, 15, 22-24</sup> In addition, intensive studies have demonstrated that the dual phase  $\text{Li}_4\text{Ti}_5\text{O}_{12}$ /anatase  $\text{TiO}_2$  composites present superior electrochemical performance than pure  $\text{Li}_4\text{Ti}_5\text{O}_{12}$ . During the dual phase structure, the higher theoretical specific capacity of anatase  $\text{TiO}_2$  ( $336 \text{ mAh g}^{-1}$ ) compared with that of spinel  $\text{Li}_4\text{Ti}_5\text{O}_{12}$  ( $175 \text{ mAh g}^{-1}$ ) and the interfacial pseudocapacitive effect derived from abundant phase interfaces between spinel  $\text{Li}_4\text{Ti}_5\text{O}_{12}$  and anatase  $\text{TiO}_2$  make contribution to the improved specific capacity of  $\text{Li}_4\text{Ti}_5\text{O}_{12}/\text{TiO}_2$  composite. Moreover, the lithium insertion/extraction ability of the  $\text{Li}_4\text{Ti}_5\text{O}_{12}/\text{TiO}_2$  composite can be enhanced by phase interfaces and nanosized anatase  $\text{TiO}_2$ .<sup>12, 16, 23, 25-28</sup> Based on the above discussions, it is attractive to design a novel  $\text{Li}_4\text{Ti}_5\text{O}_{12}$  material with the merits of nanoscale structure, abundant phase interfaces

and decorating with carbon material.

In this work, we report a facile sol-gel route with a subsequent heat treatment to fabricate  $\text{Li}_4\text{Ti}_5\text{O}_{12}/\text{TiO}_2/\text{C}$  nanocrystalline composite. The structure and electrochemical performance of the as-prepared  $\text{Li}_4\text{Ti}_5\text{O}_{12}/\text{TiO}_2/\text{C}$  composite are investigated in detail. The resultant  $\text{Li}_4\text{Ti}_5\text{O}_{12}/\text{TiO}_2/\text{C}$  composite displays a superior rate capability and cycle stability in comparison with pure  $\text{Li}_4\text{Ti}_5\text{O}_{12}$ ,  $\text{Li}_4\text{Ti}_5\text{O}_{12}/\text{C}$  and  $\text{Li}_4\text{Ti}_5\text{O}_{12}/\text{TiO}_2$  composites. The improved electrochemical performance could be attributed to the synergetic effect of uniform nanocrystalline structure, plentiful grain boundaries and phase interfaces, and *in situ* formed carbon.

## Experimental

### Materials synthesis

Tetrabutyl titanate ( $\text{Ti}(\text{OC}_4\text{H}_9)_4$ , TBOT, Aladdin) and lithium acetate dihydrate ( $\text{CH}_3\text{COOLi}\cdot 2\text{H}_2\text{O}$ , LiAc, Sinopharm Chemical Reagent Co., Ltd (China)) were utilized as titanium and lithium sources, respectively. Mixture of distilled water ( $\text{H}_2\text{O}$ ) and ethanol (EtOH, 99.5%) was used as the solvent. Glacial acetic acid (HAc, Sinopharm Chemical Reagent Co., Ltd (China)) was used as catalyst for gelation. Poly(vinylpyrrolidone) (PVP, Sigma-Aldrich,  $M_w=10,000$ ) was used as a phase separation inducer. All chemicals were of analytical grade and used as received without further purification.

The whole fabrication procedure is shown in Fig. 1. In a typical synthesis, with the molar ratio of Li/Ti at 3.8:5, 1.5 mL (4.4 mM) TBOT and a certain amount of  $\text{LiAc}\cdot 2\text{H}_2\text{O}$  were dissolved in 2.5 mL EtOH to obtain transparent solution A. 0.25

mL HAc, 0.3 mL deionized water and 2.0 mL EtOH were mixed, then 0.75 g PVP was added and stirred at room temperature about 30 min to gain pale yellow solution B. Then, the solution B was slowly dropped into the solution A under vigorous stirring. After continuously stirring for 5 min, the mix solution was kept in a sealed container at 60 °C for gelation, and white gels could be acquired after about 20 min. The colour of the gel was changed from white to light orange during the drying process. After dried at 80 °C for 2 d, the resulting dried gels were calcinated at 600 °C for 5 h in air and an argon atmosphere to obtain  $\text{Li}_4\text{Ti}_5\text{O}_{12}/\text{TiO}_2$  and  $\text{Li}_4\text{Ti}_5\text{O}_{12}/\text{TiO}_2/\text{C}$  composites, respectively. For comparison, the pure  $\text{Li}_4\text{Ti}_5\text{O}_{12}$  and the  $\text{Li}_4\text{Ti}_5\text{O}_{12}/\text{C}$  composite were also prepared with the molar stoichiometric ratio of Li/Ti (4:5) after the calcination at 600 °C for 5 h in air and an argon atmosphere, respectively.

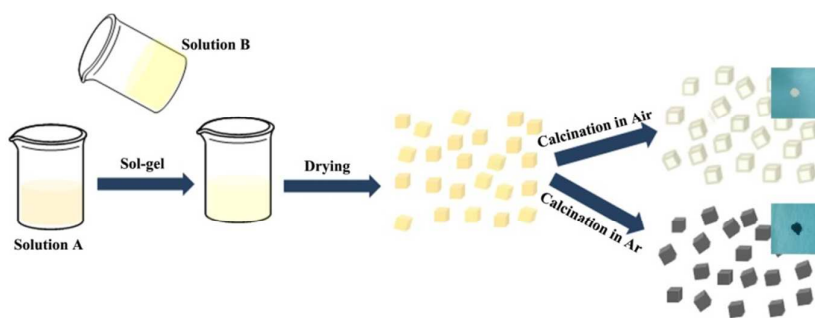


Fig. 1 Schematic illustration of the fabrication process of pure  $\text{Li}_4\text{Ti}_5\text{O}_{12}$ ,  $\text{Li}_4\text{Ti}_5\text{O}_{12}/\text{C}$ ,  $\text{Li}_4\text{Ti}_5\text{O}_{12}/\text{TiO}_2$  and  $\text{Li}_4\text{Ti}_5\text{O}_{12}/\text{TiO}_2/\text{C}$  composites (insets are the corresponding optical photographs).

### Structure characterizations

The phase purity and crystal structure of as-obtained products were characterized using powder X-ray diffractometry (XRD; X'Pert Pro diffractometer with a Cu K $\alpha$  radiation,  $\lambda = 0.15418$  nm). Morphology and microstructure were determined by scanning electron microscopy (SEM; Hitachi S-4800) and transmission electron

microscopy (TEM; FEI, Tecnai G2 F20). The chemical valence state of elements for the samples was studied by X-ray photoelectron spectroscopy (XPS) performed on a Thermo ESCALAB 250 system with a monochromatic Al-K $\alpha$  (1486.6 eV) as the X-ray source. Measurements of Raman spectra were collected on a Renishaw InVia Raman Spectrometer under a backscattering geometry ( $\lambda = 532$  nm). The thermal decomposition behavior of the dried gel and the amount of carbon in the composites were examined by thermogravimetric analysis (TGA, TA Q500) at a heating rate of 10 °C min<sup>-1</sup> from room temperature to 800 °C in air.

### **Electrochemical measurements**

Electrochemical experiments were evaluated using standard CR 2025 type coin cells with lithium foil as the counter and reference electrodes. Active material (as-prepared samples), conductive super P and polyvinylidene fluoride (PVDF) binder were mixed at a weight ratio of 80:10:10 in N-methyl-2-pyrrolidone (NMP) solution to form a slurry. The slurry was homogeneously coated onto a Cu foil and dried in a vacuum oven at 120 °C for 12 h before coin-cell assembly. The weight of the active material in the electrode sheet was 2~3 mg cm<sup>-2</sup>. A solution of 1M LiPF<sub>6</sub> dissolved in a mixture of ethylene carbonate (EC)/dimethyl carbonate (DMC) (1:1 by volume) was used as the electrolyte, and a polypropylene (PP) microporous film (Cellgard 2300) as the separator. Galvanostatic charge-discharge measurements were performed on a Neware battery test system in the voltage range of 1.0-3.0 V at room temperature. A CHI 660b workstation (Shanghai Chenhua, China) was applied for cyclic voltammograms (CV) tests in the voltage range of 1.0-3.0 V at a

scan rate of  $0.1 \text{ mV s}^{-1}$ . The electrochemical impedance spectroscopy (EIS) measurements were collected on the same workstation over the frequency range 0.1 Hz to 100 KHz with a voltage amplitude of 5.0 mV.

## Results and discussion

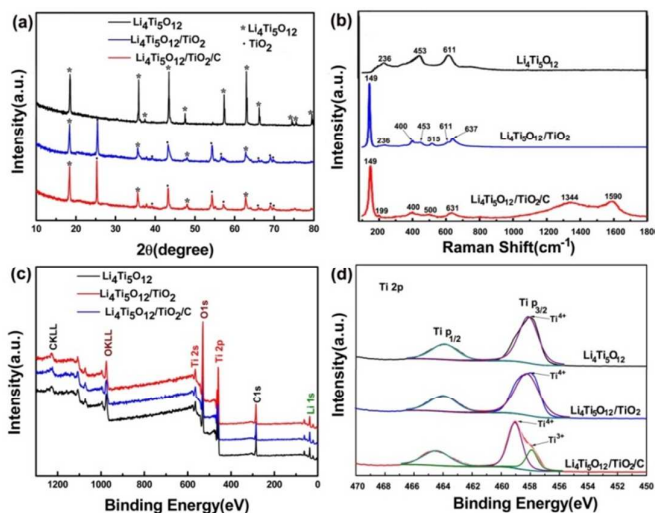


Fig. 2 XRD patterns (a), Raman spectra (b), Full XPS survey spectra (c) and high-resolution Ti 2p spectra (d) of pure  $\text{Li}_4\text{Ti}_5\text{O}_{12}$ ,  $\text{Li}_4\text{Ti}_5\text{O}_{12}/\text{TiO}_2$  and  $\text{Li}_4\text{Ti}_5\text{O}_{12}/\text{TiO}_2/\text{C}$  composites, respectively.

Fig. 2a shows the XRD patterns of the as-prepared products. It can be seen that all the samples present sharp peaks, indicating that all the samples are well crystallized after calcination at a relatively low temperature of  $600 \text{ }^\circ\text{C}$ . Pure  $\text{Li}_4\text{Ti}_5\text{O}_{12}$  phase can be obtained in the pure  $\text{Li}_4\text{Ti}_5\text{O}_{12}$  and  $\text{Li}_4\text{Ti}_5\text{O}_{12}/\text{C}$  composite (Fig.S1), and all the diffraction peaks are consistent with the cubic spinel phase  $\text{Li}_4\text{Ti}_5\text{O}_{12}$  (JCPDS No. 49-0207) without any impurities. The  $\text{Li}_4\text{Ti}_5\text{O}_{12}/\text{TiO}_2$  and  $\text{Li}_4\text{Ti}_5\text{O}_{12}/\text{TiO}_2/\text{C}$  composites can be obtained at the ratio of Li/Ti (3.8:5), the additional peaks marked by dot are indexed to anatase  $\text{TiO}_2$  (JCPDS 65-5714). No obvious broad peaks corresponding to amorphous or crystalline carbon can be found against the background in the XRD pattern of  $\text{Li}_4\text{Ti}_5\text{O}_{12}/\text{C}$  (Fig. S1) and

Li<sub>4</sub>Ti<sub>5</sub>O<sub>12</sub>/TiO<sub>2</sub>/C composites, which could be attributed to the low crystallinity and the combination mode of the carbon.<sup>5, 7, 23, 24, 29</sup> However, the carbon composition of Li<sub>4</sub>Ti<sub>5</sub>O<sub>12</sub>/TiO<sub>2</sub>/C composite can be confirmed by Raman spectrum (Fig. 2b) and TEM examination (described later).

The phase compositions of the as-obtained samples are further studied by Raman spectrum shown in Fig. 2b. The observed peaks at 236, 453 and 611 cm<sup>-1</sup>, corresponding to the characteristic peaks of spinel Li<sub>4</sub>Ti<sub>5</sub>O<sub>12</sub>.<sup>9, 30</sup> Besides, the typical vibration peaks of anatase TiO<sub>2</sub> located at 149, 199, 400, 500, 515, 631 and 637 cm<sup>-1</sup> are found for the samples of Li<sub>4</sub>Ti<sub>5</sub>O<sub>12</sub>/TiO<sub>2</sub> and Li<sub>4</sub>Ti<sub>5</sub>O<sub>12</sub>/TiO<sub>2</sub>/C composites.<sup>7, 31</sup> Furthermore, two peaks at 1344 and 1590 cm<sup>-1</sup> are observed for the Li<sub>4</sub>Ti<sub>5</sub>O<sub>12</sub>/TiO<sub>2</sub>/C composite, which are attributed to the typical disordered band (D band) and the graphene band (G band) of carbon, respectively.<sup>10, 13, 32</sup> The compositions (Li<sub>4</sub>Ti<sub>5</sub>O<sub>12</sub> and carbon) of the Li<sub>4</sub>Ti<sub>5</sub>O<sub>12</sub> /C composite are also confirmed by the Raman spectrum (Fig.S2). The result of Raman spectra indicates that the existence of carbon, which results from the *in situ* formed carbon derived from the pyrolysis of PVP in an argon atmosphere.<sup>7</sup> Moreover, the  $I_G/I_D$  value (ratio of the intensity of G Raman peak and D Raman peak) is about 0.96, indicating that the carbon is mainly exist as disordered form with low crystallinity, which is agree with the results of XRD.

Further surface chemical compositions and elemental states of the as-prepared samples were collected *via* X-ray photoelectron spectroscopy (XPS). The binding energies obtained in the XPS spectrum were corrected with reference to the C 1s

peak at 284.6 eV. As shown in Fig. 2c, obvious peaks of O1s, Ti2p, N1s, C1s and Li1s peaks are observed for all the samples, indicating the existence of these elements. Fig. 2d shows the high resolution spectra of the Ti2p, the typical Ti2p<sub>1/2</sub> and Ti2p<sub>3/2</sub> of Ti<sup>4+</sup> located at 463.8 and 458.0 eV can be detected from the pure Li<sub>4</sub>Ti<sub>5</sub>O<sub>12</sub>.<sup>7, 15</sup> The Li<sub>4</sub>Ti<sub>5</sub>O<sub>12</sub>/TiO<sub>2</sub> and Li<sub>4</sub>Ti<sub>5</sub>O<sub>12</sub>/TiO<sub>2</sub>/C composites also present similar Ti2p<sub>1/2</sub> and Ti2p<sub>3/2</sub> characteristic peaks, and the peaks of Ti 2p<sub>1/2</sub> and Ti 2p<sub>3/2</sub> migrate to higher binding energy compared with pure Li<sub>4</sub>Ti<sub>5</sub>O<sub>12</sub>. This phenomenon is obvious for the Li<sub>4</sub>Ti<sub>5</sub>O<sub>12</sub>/TiO<sub>2</sub>/C composite. Moreover, the characteristic peak of Ti<sup>3+</sup> at 457.6 eV is observed for the Li<sub>4</sub>Ti<sub>5</sub>O<sub>12</sub>/TiO<sub>2</sub>/C composite, which may be attributed to the increased oxygen vacancies in the Li<sub>4</sub>Ti<sub>5</sub>O<sub>12</sub>/TiO<sub>2</sub>/C composite due to the reduction effect derived from the argon atmosphere and *in-situ* formed carbon.<sup>15, 33</sup> The existence of Ti<sup>3+</sup> and oxygen vacancies is favorable to enhancing Li<sup>+</sup> insertion and increasing electronic conductivity, which are beneficial to improving electrochemical performance of the Li<sub>4</sub>Ti<sub>5</sub>O<sub>12</sub>/TiO<sub>2</sub>/C composite.

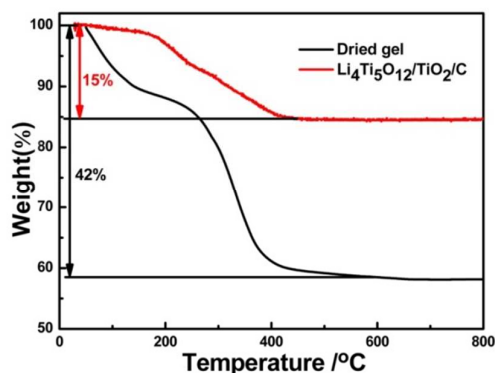


Fig. 3 TG curves of the as-prepared dried gel and the Li<sub>4</sub>Ti<sub>5</sub>O<sub>12</sub>/TiO<sub>2</sub>/C composite.

Thermal analysis was used to analyze the thermal behavior of the dried gel and actual carbon content of Li<sub>4</sub>Ti<sub>5</sub>O<sub>12</sub>/C and Li<sub>4</sub>Ti<sub>5</sub>O<sub>12</sub>/TiO<sub>2</sub>/C composites. As shown in

Fig. 3, for dried gel, there is a small weight loss of about 10% happened up to 120 °C, which is mainly due to the elimination of absorbed/trapped water contained in the sample. Subsequently, there is a distinct weight loss of about 32% occurred from 120 to 600 °C, which can be attributed to the chemical reaction of dried gel and the decomposition of PVP residue. Additionally, the distinct weight loss of  $\text{Li}_4\text{Ti}_5\text{O}_{12}/\text{TiO}_2/\text{C}$  composite is observed between 200 and 500 °C, which is ascribed to the decomposition of carbon and calculated to be 15%. That is to say, the carbon content of  $\text{Li}_4\text{Ti}_5\text{O}_{12}/\text{TiO}_2/\text{C}$  composite is about 15%. Similar results are observed from the  $\text{Li}_4\text{Ti}_5\text{O}_{12}/\text{C}$  composite (Fig. S3), and the carbon content of  $\text{Li}_4\text{Ti}_5\text{O}_{12}/\text{C}$  composite is 15.6 %.

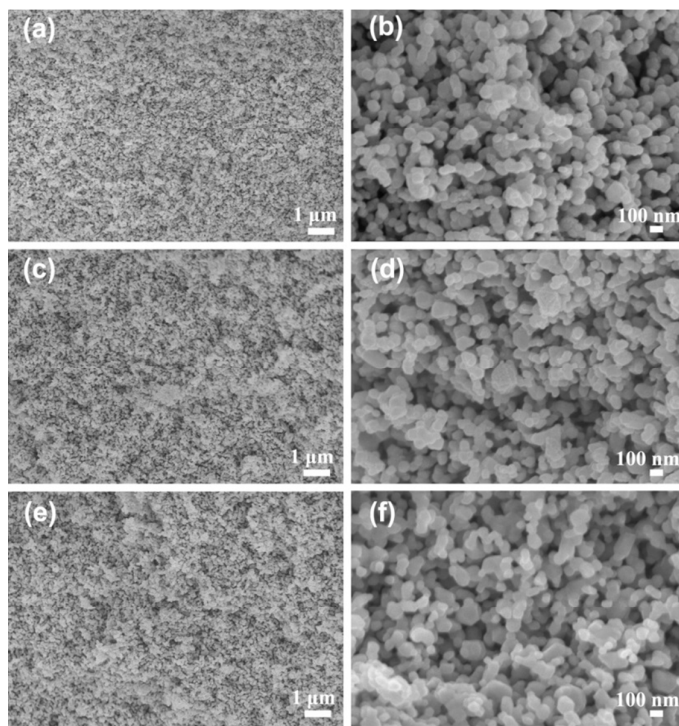


Fig. 4 Typical low-magnification and high-magnification SEM images of pure  $\text{Li}_4\text{Ti}_5\text{O}_{12}$  (a and b),  $\text{Li}_4\text{Ti}_5\text{O}_{12}/\text{TiO}_2$  (c and d) and  $\text{Li}_4\text{Ti}_5\text{O}_{12}/\text{TiO}_2/\text{C}$  composites (e and f).

The morphology of the products was characterized by SEM. As shown in Fig.4

and Fig. S4, it can be observed from the low-magnification images (Fig. 4 a, c, e and Fig. S4a) that all the samples present a similar morphology composed of uniform nanocrystalline particles due to the surfactant and phase separation induction effect of PVP.<sup>7</sup> The high-magnification images (Fig. 4 b, d, f and Fig. S4b) show that homogeneous nanocrystalline particles for all the samples display a similar size in the range of 50-100 nm, indicating that the second phase of anatase TiO<sub>2</sub> and carbon have no effect on the size of particles.

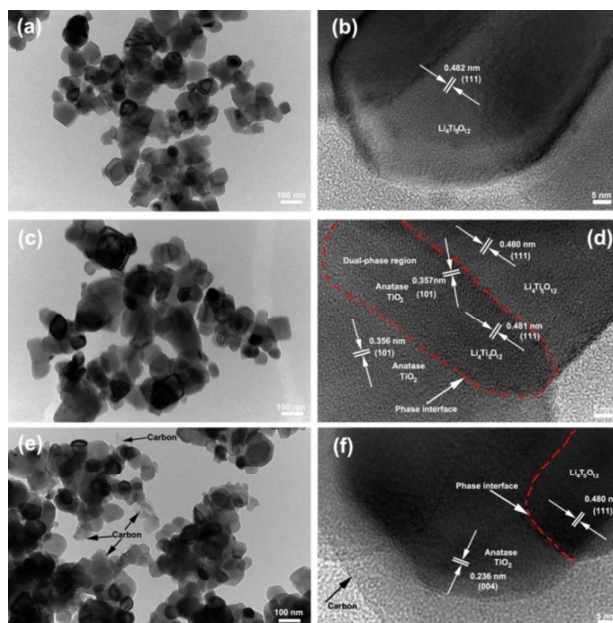


Fig.5 TEM and HRTEM images of pure Li<sub>4</sub>Ti<sub>5</sub>O<sub>12</sub> (a and b), Li<sub>4</sub>Ti<sub>5</sub>O<sub>12</sub>/TiO<sub>2</sub> (c and d), and Li<sub>4</sub>Ti<sub>5</sub>O<sub>12</sub>/TiO<sub>2</sub>/C composites (e and f).

TEM and HRTEM were performed to further study the microstructure and carbon distribution (Fig. 5). Agree with the SEM images (Fig. 4), all the samples present a nanocrystalline structure (Fig. 5a, c and e). These nanoparticles interconnect into a network porous structure, which is beneficial to enhancing the electrochemical performances. Furthermore, the dispersion of carbon can be found

in the  $\text{Li}_4\text{Ti}_5\text{O}_{12}/\text{TiO}_2/\text{C}$  composite, as marked by the arrows in Fig. 5e. The lattice spacing of 0.482 nm in Fig. 5b corresponds to the (111) crystal plane of spinel  $\text{Li}_4\text{Ti}_5\text{O}_{12}$ . Compared with pure  $\text{Li}_4\text{Ti}_5\text{O}_{12}$ , the characteristic lattice stripes of anatase  $\text{TiO}_2$  can be detected from the  $\text{Li}_4\text{Ti}_5\text{O}_{12}/\text{TiO}_2$  and  $\text{Li}_4\text{Ti}_5\text{O}_{12}/\text{TiO}_2/\text{C}$  composites in Fig. 5d and f. The lattice spacing values of 0.356/0.357 and 0.236 nm are assigned to the (101) and (004) planes of anatase  $\text{TiO}_2$ , respectively. Abundant grain boundaries and phase interfaces are produced due to nanocrystal components and dual-phase of  $\text{Li}_4\text{Ti}_5\text{O}_{12}$  and anatase  $\text{TiO}_2$ , as marked by the red dashed line in Fig. 5d and f. Besides, the grey regions marked by black arrow in Fig. 5f could be detected from the  $\text{Li}_4\text{Ti}_5\text{O}_{12}/\text{TiO}_2/\text{C}$  composite, which could be attributed to the *in situ* formed carbon derived from PVP. The high crystallinity of the as-obtained samples can be further confirmed by the distinct lattice stripes in the HRTEM images (Fig. 5b, d and f), which is consistent with the results of XRD shown above.

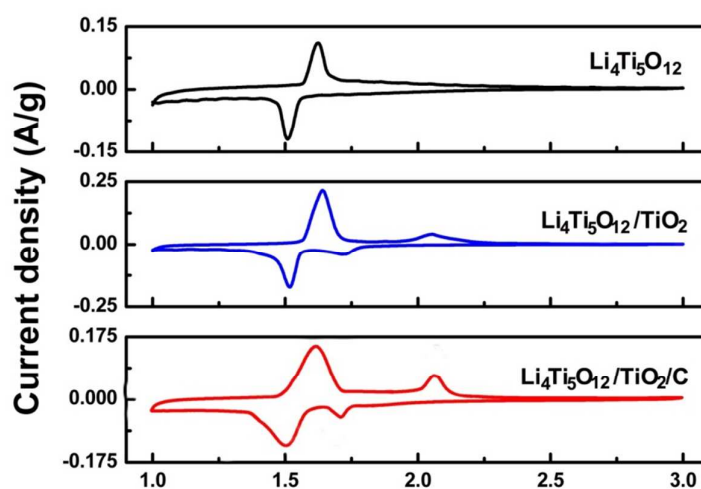


Fig. 6 CV curves of pure  $\text{Li}_4\text{Ti}_5\text{O}_{12}$ ,  $\text{Li}_4\text{Ti}_5\text{O}_{12}/\text{TiO}_2$  and  $\text{Li}_4\text{Ti}_5\text{O}_{12}/\text{TiO}_2/\text{C}$  composites.

The electrochemical behaviour of pure  $\text{Li}_4\text{Ti}_5\text{O}_{12}$ ,  $\text{Li}_4\text{Ti}_5\text{O}_{12}/\text{C}$ ,  $\text{Li}_4\text{Ti}_5\text{O}_{12}/\text{TiO}_2$  and  $\text{Li}_4\text{Ti}_5\text{O}_{12}/\text{TiO}_2/\text{C}$  composite electrodes was characterized by cyclic voltammetry (CV) at a scanning rate of  $0.1 \text{ mV s}^{-1}$  in the potential range of 1.0-3.0 V, as shown in Fig. 6. Only one oxidation/reduction peak at 1.51 and 1.62 V is observed for the pure  $\text{Li}_4\text{Ti}_5\text{O}_{12}$  and the  $\text{Li}_4\text{Ti}_5\text{O}_{12}/\text{C}$  composite (Fig. S5) electrode, corresponding to the  $\text{Li}^+$  insertion/extraction reaction of spinel  $\text{Li}_4\text{Ti}_5\text{O}_{12}$  ( $\text{Li}_4\text{Ti}_5\text{O}_{12} + 3\text{Li}^+ + 3\text{e}^- \leftrightarrow \text{Li}_7\text{Ti}_5\text{O}_{12}$ ).<sup>5, 9, 34</sup> Besides, an additional pair of redox peaks located at 1.72/2.04 V is detected for the  $\text{Li}_4\text{Ti}_5\text{O}_{12}/\text{TiO}_2$  and  $\text{Li}_4\text{Ti}_5\text{O}_{12}/\text{TiO}_2/\text{C}$  composites, which is attributed to the discharge and charge plateaus of anatase  $\text{TiO}_2$  phase ( $x\text{Li}^+ + \text{TiO}_2 + x\text{e}^- \leftrightarrow \text{Li}_x\text{TiO}_2$ ).<sup>7, 9, 35</sup> It can be detected that the background of the redox peaks for  $\text{Li}_4\text{Ti}_5\text{O}_{12}/\text{C}$  (Fig. S5) and  $\text{Li}_4\text{Ti}_5\text{O}_{12}/\text{TiO}_2/\text{C}$  composites is much more wider than that of pure  $\text{Li}_4\text{Ti}_5\text{O}_{12}$  and  $\text{Li}_4\text{Ti}_5\text{O}_{12}/\text{TiO}_2$  composite, which can be assigned to the pseudocapacitive of the faradaic-limited process derived from the carbon.<sup>7, 36</sup>

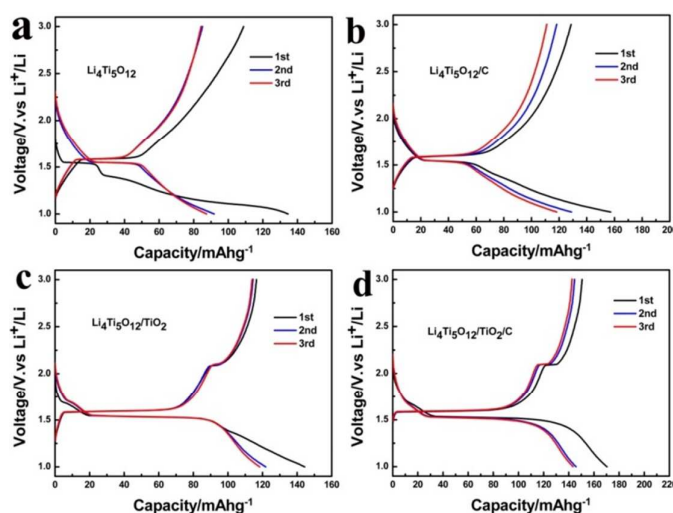


Fig. 7 Initial three discharge/charge curves of (a) pure  $\text{Li}_4\text{Ti}_5\text{O}_{12}$ , (b)  $\text{Li}_4\text{Ti}_5\text{O}_{12}/\text{C}$ , (c)  $\text{Li}_4\text{Ti}_5\text{O}_{12}/\text{TiO}_2$  and (d)  $\text{Li}_4\text{Ti}_5\text{O}_{12}/\text{TiO}_2/\text{C}$  composites, respectively.

As is well known, the volumic capacity is an important parameter for the practical application of  $\text{Li}_4\text{Ti}_5\text{O}_{12}$ -based materials<sup>37, 38</sup>. The capacities of the samples in this work are addressed not only by weight dimensionality ( $\text{mAh g}^{-1}$ ) but also by volume ( $\text{mAh cm}^{-3}$ ). The densities of the pure  $\text{Li}_4\text{Ti}_5\text{O}_{12}$ ,  $\text{Li}_4\text{Ti}_5\text{O}_{12}/\text{C}$ ,  $\text{Li}_4\text{Ti}_5\text{O}_{12}/\text{TiO}_2$  and  $\text{Li}_4\text{Ti}_5\text{O}_{12}/\text{TiO}_2/\text{C}$  composites are calculated to be 3.41, 2.97, 3.52 and  $3.26 \text{ g cm}^{-3}$ , respectively. The initial three charge-discharge cycle profiles for pure  $\text{Li}_4\text{Ti}_5\text{O}_{12}$ ,  $\text{Li}_4\text{Ti}_5\text{O}_{12}/\text{C}$ ,  $\text{Li}_4\text{Ti}_5\text{O}_{12}/\text{TiO}_2$  and  $\text{Li}_4\text{Ti}_5\text{O}_{12}/\text{TiO}_2/\text{C}$  composite electrodes with a current rate of 0.5 C (1 C =  $175 \text{ mA g}^{-1}$ ) are shown in Fig 7a-d. Agree well with the result of CV curves (Fig. 6), two long flat plateaus at about 1.51 and 1.62 V are observed for all the samples due to the typical lithium insertion/extraction processes of  $\text{Li}_4\text{Ti}_5\text{O}_{12}$ . Moreover, the voltage plateaus at around 1.98 and 1.72 V are verified as the lithium ion insertion/extraction reaction of anatase  $\text{TiO}_2$ .<sup>5</sup> The initial discharge capacities of pure  $\text{Li}_4\text{Ti}_5\text{O}_{12}$ ,  $\text{Li}_4\text{Ti}_5\text{O}_{12}/\text{C}$ ,  $\text{Li}_4\text{Ti}_5\text{O}_{12}/\text{TiO}_2$  and  $\text{Li}_4\text{Ti}_5\text{O}_{12}/\text{TiO}_2/\text{C}$  composites are 134, 157, 144 and 170  $\text{mAh g}^{-1}$ , corresponding to 455, 466, 506 and  $554 \text{ mAh cm}^{-3}$ , respectively. The charge-discharge profiles of all samples are nearly invariable after the second cycle. The reversible capacities of the third cycle for pure  $\text{Li}_4\text{Ti}_5\text{O}_{12}$ ,  $\text{Li}_4\text{Ti}_5\text{O}_{12}/\text{C}$ ,  $\text{Li}_4\text{Ti}_5\text{O}_{12}/\text{TiO}_2$  and  $\text{Li}_4\text{Ti}_5\text{O}_{12}/\text{TiO}_2/\text{C}$  composites are approximately 87, 119, 117 and  $143 \text{ mAh g}^{-1}$ , corresponding to 297, 353, 411 and  $466 \text{ mAh cm}^{-3}$ , respectively. The higher specific capacity of  $\text{Li}_4\text{Ti}_5\text{O}_{12}/\text{TiO}_2/\text{C}$  composite is contributed by relatively high theoretical capacity of anatase  $\text{TiO}_2$  and carbon, and the extra lithium storage derived from phase interfaces.

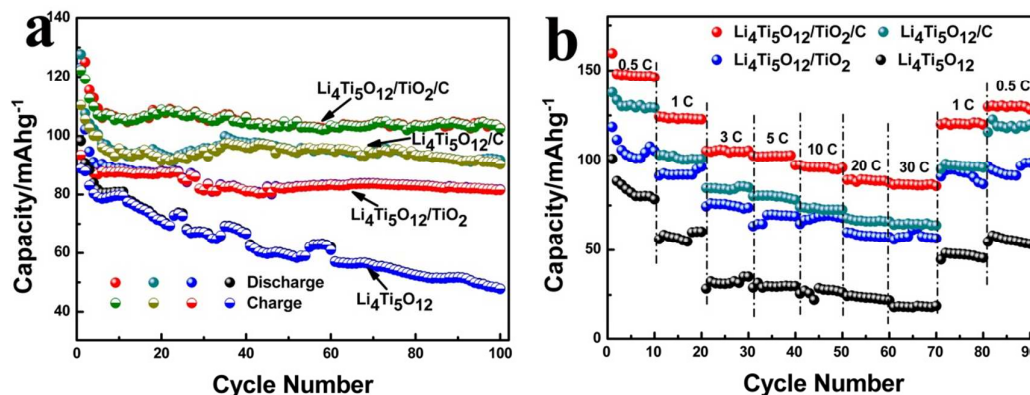


Fig. 8 (a) Cycling performance at 1 C and (b) Rate performance (from 0.5 C to 30 C and back to 0.5 C) of pure  $\text{Li}_4\text{Ti}_5\text{O}_{12}$ ,  $\text{Li}_4\text{Ti}_5\text{O}_{12}/\text{C}$ ,  $\text{Li}_4\text{Ti}_5\text{O}_{12}/\text{TiO}_2$  and  $\text{Li}_4\text{Ti}_5\text{O}_{12}/\text{TiO}_2/\text{C}$  composites, respectively.

Fig. 8a compares the cyclic stability of the  $\text{Li}_4\text{Ti}_5\text{O}_{12}/\text{TiO}_2/\text{C}$  composite at 1 C with that of pure  $\text{Li}_4\text{Ti}_5\text{O}_{12}$ ,  $\text{Li}_4\text{Ti}_5\text{O}_{12}/\text{C}$  and  $\text{Li}_4\text{Ti}_5\text{O}_{12}/\text{TiO}_2$  composites in the voltage range of 1.0-3.0 V. It can be observed that the  $\text{Li}_4\text{Ti}_5\text{O}_{12}/\text{TiO}_2/\text{C}$  composite electrode displays a higher capacity and better cycling performance compared with pure  $\text{Li}_4\text{Ti}_5\text{O}_{12}$ ,  $\text{Li}_4\text{Ti}_5\text{O}_{12}/\text{C}$  and  $\text{Li}_4\text{Ti}_5\text{O}_{12}/\text{TiO}_2$  composites. Moreover, it is noted that the reversible capacities of  $\text{Li}_4\text{Ti}_5\text{O}_{12}/\text{C}$  and  $\text{Li}_4\text{Ti}_5\text{O}_{12}/\text{TiO}_2/\text{C}$  composites display an upward trend during the early cycles, this phenomena is commonly observed from the carbon-based composites, which may imply that more diffusion paths are created through the carbon.<sup>39-41</sup> After 100 cycles, the reversible capacity of the  $\text{Li}_4\text{Ti}_5\text{O}_{12}/\text{TiO}_2/\text{C}$  composite is measured to be  $102 \text{ mAh g}^{-1}$  ( $333 \text{ mAh cm}^{-3}$ ) with a high cycle stability, which is about 80 % of the initial capacity. On the contrary, the reversible capacities for pure  $\text{Li}_4\text{Ti}_5\text{O}_{12}$ ,  $\text{Li}_4\text{Ti}_5\text{O}_{12}/\text{C}$  and  $\text{Li}_4\text{Ti}_5\text{O}_{12}/\text{TiO}_2$  composite electrodes are only 47, 90 and 81  $\text{mAh g}^{-1}$ , corresponding to 160, 267, and 264  $\text{mAh cm}^{-3}$ , respectively.

The cell was progressively charged and discharged at various rates from 0.5 C

to 30 C for 10 cycles, and then again at 1 and 0.5 C for 10 cycles. It can be detected in Fig. 8b that the  $\text{Li}_4\text{Ti}_5\text{O}_{12}/\text{TiO}_2/\text{C}$  composite presents the best rate capability, the result is consistent with Fig. 8a. Compared with pure  $\text{Li}_4\text{Ti}_5\text{O}_{12}$ ,  $\text{Li}_4\text{Ti}_5\text{O}_{12}/\text{C}$  and  $\text{Li}_4\text{Ti}_5\text{O}_{12}/\text{TiO}_2$  composites, it can be observed that the  $\text{Li}_4\text{Ti}_5\text{O}_{12}/\text{TiO}_2/\text{C}$  composite shows a slower capacity decay with the increase of C-rates, especially at high rates. A high capacity of  $88 \text{ mAh g}^{-1}$  ( $286 \text{ mAh cm}^{-3}$ ) can be achieved for the  $\text{Li}_4\text{Ti}_5\text{O}_{12}/\text{TiO}_2/\text{C}$  composite at the high rate of 30 C, whereas the value drops to only 17, 68 and  $54 \text{ mAh g}^{-1}$  for the pure  $\text{Li}_4\text{Ti}_5\text{O}_{12}$ ,  $\text{Li}_4\text{Ti}_5\text{O}_{12}/\text{C}$  and  $\text{Li}_4\text{Ti}_5\text{O}_{12}/\text{TiO}_2$  composites at the same rate, and the corresponding volumic capacities are 60, 202 and  $190 \text{ mAh cm}^{-3}$ , respectively. It can be found that the  $\text{Li}_4\text{Ti}_5\text{O}_{12}/\text{TiO}_2/\text{C}$  composite presents the highest specific capacity both in  $\text{mAh g}^{-1}$  and  $\text{mAh cm}^{-3}$ . The significantly improved rate capability of the  $\text{Li}_4\text{Ti}_5\text{O}_{12}/\text{TiO}_2/\text{C}$  composite is attributed to the improved electrical conductivity contributed by the *in situ* formed carbon, anatase  $\text{TiO}_2$  and phase interfaces. Moreover, when the current density is returned to 1 and 0.5 C again, specific capacities of the samples except the pure  $\text{Li}_4\text{Ti}_5\text{O}_{12}$  can be recovered to a large extent, which could be attributed to the improved lithium insertion/extraction kinetics and the enhanced structure stability guaranteed by the abundant phase interfaces and the *in situ* formed carbon. It is noted that the specific capacities are calculated based on the weight of the whole composites in this work. According to the content of about 15% in the TG curve (Fig. 3 and Fig. S3) and a theoretical specific capacity of  $372 \text{ mAh g}^{-1}$ , the specific capacity contributed by the carbon

for  $\text{Li}_4\text{Ti}_5\text{O}_{12}/\text{C}$  and  $\text{Li}_4\text{Ti}_5\text{O}_{12}/\text{TiO}_2/\text{C}$  composites is calculated to be  $55.8 \text{ mAh g}^{-1}$  ( $127 \text{ mAh cm}^{-3}$ ). Actually, the actual value is less than that due to the low crystallinity and irregular *in situ* combination mode. Although the specificities of  $\text{Li}_4\text{Ti}_5\text{O}_{12}/\text{C}$  and  $\text{Li}_4\text{Ti}_5\text{O}_{12}/\text{TiO}_2/\text{C}$  composites do not exhibit a large increase compared with the pure  $\text{Li}_4\text{Ti}_5\text{O}_{12}$  and  $\text{Li}_4\text{Ti}_5\text{O}_{12}/\text{TiO}_2$  composite, a more stable cycle curves (Fig. 8 a and b) can be observed for  $\text{Li}_4\text{Ti}_5\text{O}_{12}/\text{C}$  and  $\text{Li}_4\text{Ti}_5\text{O}_{12}/\text{TiO}_2/\text{C}$  composites, which is contributed by the high electrical conductivity of the *in situ* formed carbon.

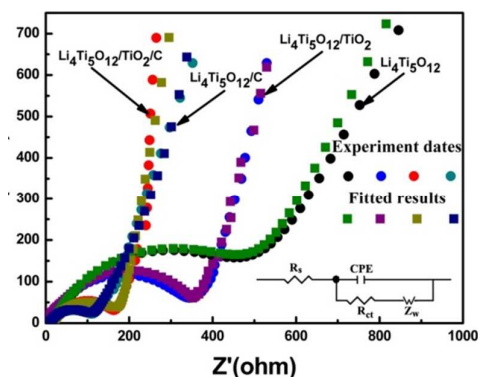


Fig. 9 Electrochemical impedance spectra (Nyquist plots) and corresponding simulation results of pure  $\text{Li}_4\text{Ti}_5\text{O}_{12}$ ,  $\text{Li}_4\text{Ti}_5\text{O}_{12}/\text{C}$ ,  $\text{Li}_4\text{Ti}_5\text{O}_{12}/\text{TiO}_2$  and  $\text{Li}_4\text{Ti}_5\text{O}_{12}/\text{TiO}_2/\text{C}$  composites, respectively. The inset is the equivalent circuit used for plots fitting.

Electrochemical impedance spectroscopy (EIS) measurement was performed, and the corresponding Nyquist plots are displayed in Fig. 9. All the Nyquist plots exhibit one semicircle in the high frequency range and a sloping straight line in the low frequency range. The diameter of the semicircle is mainly related to the surface charge transfer resistance ( $R_{ct}$ ), associated with the interfacial electrochemical reaction activity, and the sloping straight line in low frequency region corresponds to the lithium ion diffusion process in the electrodes.<sup>2, 8, 15</sup> Nyquist plots are fitted using the equivalent circuit (inset of Fig. 9). In this equivalent circuit,  $R_s$  is the electrode

resistance,  $R_{ct}$  is the charge-transfer resistance, CPE is the double layer capacitance and  $Z_w$  represents the Warburg impedance.

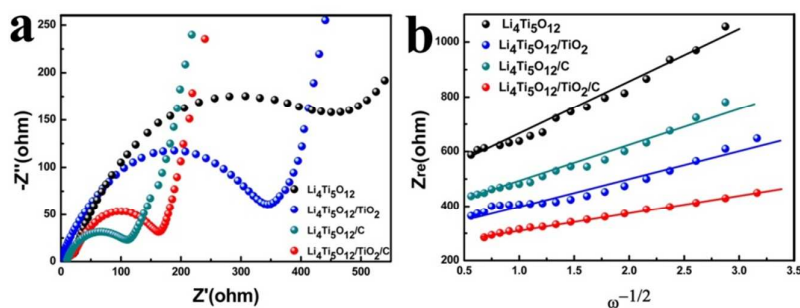


Fig. 10 (a) Enlarged Nyquist plots at high frequency region and (b) Graph of  $Z_{re}$  plotted against  $\omega^{-1/2}$  at low frequency region of pure  $\text{Li}_4\text{Ti}_5\text{O}_{12}$ ,  $\text{Li}_4\text{Ti}_5\text{O}_{12}/\text{C}$ ,  $\text{Li}_4\text{Ti}_5\text{O}_{12}/\text{TiO}_2$  and  $\text{Li}_4\text{Ti}_5\text{O}_{12}/\text{TiO}_2/\text{C}$  composites, respectively.

Fig. 10a shows the enlarged Nyquist plots at high frequency region. It is found that the sizes of semicircles for  $\text{Li}_4\text{Ti}_5\text{O}_{12}/\text{C}$  and  $\text{Li}_4\text{Ti}_5\text{O}_{12}/\text{TiO}_2/\text{C}$  composites are smaller than that of pure  $\text{Li}_4\text{Ti}_5\text{O}_{12}$  and  $\text{Li}_4\text{Ti}_5\text{O}_{12}/\text{TiO}_2$  composite. That is to say, the  $\text{Li}_4\text{Ti}_5\text{O}_{12}/\text{C}$  and  $\text{Li}_4\text{Ti}_5\text{O}_{12}/\text{TiO}_2/\text{C}$  composites possess the smaller charge transfer resistance compared with pure  $\text{Li}_4\text{Ti}_5\text{O}_{12}$  and  $\text{Li}_4\text{Ti}_5\text{O}_{12}/\text{TiO}_2$  composite, which could be attributed to enhanced electrical conductivity derived from the *in situ* formed carbon.<sup>7, 15</sup> Moreover, the slopes in low frequency are directly proportional to the lithium ion diffusion coefficient ( $D_{\text{Li}}$ ).<sup>42-44</sup> The  $D_{\text{Li}}$  can be calculated from the plots in low frequency region according to the following equations<sup>42, 45, 46</sup>:

$$D = R^2 T^2 / 2 A^2 n^4 F^4 C_{\text{Li}}^2 \sigma^2 \quad (1)$$

$$Z_{re} = R_e + R_{ct} + \sigma \omega^{-1/2} \quad (2)$$

Where  $R$  is the gas constant,  $T$  is the absolute temperature,  $A$  is the surface area of the electrode,  $n$  is the number of electrons transferred in the half-reaction for the redox couple,  $F$  is the Faraday constant,  $C_{\text{Li}}$  is the concentration of lithium ion in

solid, and  $\sigma$  is the Warburg factor, which is relative to  $Z_{re}-\sigma$  and can be obtained from the slope of the lines in Fig. 10b. As expressed in above equations, it is clear that  $D$  is inversely proportional to  $\sigma$ . Furthermore, the slope of the linear fitting lines of  $Z_{re}$  vs.  $\omega$  is  $\sigma$ . As shown in Fig. 10b, the  $\text{Li}_4\text{Ti}_5\text{O}_{12}/\text{TiO}_2$  and  $\text{Li}_4\text{Ti}_5\text{O}_{12}/\text{TiO}_2/\text{C}$  composites have a smaller slope compared to pure  $\text{Li}_4\text{Ti}_5\text{O}_{12}$  and  $\text{Li}_4\text{Ti}_5\text{O}_{12}/\text{C}$  composite, demonstrating that a higher  $\text{Li}^+$  diffusion coefficient could be obtained for the  $\text{Li}_4\text{Ti}_5\text{O}_{12}/\text{TiO}_2$  and  $\text{Li}_4\text{Ti}_5\text{O}_{12}/\text{TiO}_2/\text{C}$  composites. The higher  $\text{Li}^+$  diffusion coefficient could be ascribed to the contribution of anatase  $\text{TiO}_2$  and the abundant phase interfaces.<sup>16, 47</sup> Meanwhile, the  $\text{Li}_4\text{Ti}_5\text{O}_{12}/\text{C}$  composite presents a smaller slope in comparison with pure  $\text{Li}_4\text{Ti}_5\text{O}_{12}$  due to the existence of  $\text{Ti}^{3+}$ . The results of EIS indicate that the  $\text{Li}_4\text{Ti}_5\text{O}_{12}/\text{TiO}_2/\text{C}$  composite possesses higher charge transfer kinetics and ionic mobility derived from large number of grain boundaries and phase interfaces, and *in-situ* formed carbon, which could well explain the better electrochemical performance of the  $\text{Li}_4\text{Ti}_5\text{O}_{12}/\text{TiO}_2/\text{C}$  composite.

The  $\text{Li}_4\text{Ti}_5\text{O}_{12}/\text{TiO}_2/\text{C}$  nanocrystalline composite reported here presents excellent rate capability and cycling stability, which are compared favourably to other  $\text{Li}_4\text{Ti}_5\text{O}_{12}/\text{TiO}_2/\text{C}$  composites and  $\text{Li}_4\text{Ti}_5\text{O}_{12}/\text{TiO}_2$  based electrodes reported in the literatures.<sup>8, 15, 23, 48, 49</sup> The superior electrochemical performance of the  $\text{Li}_4\text{Ti}_5\text{O}_{12}/\text{TiO}_2/\text{C}$  nanocrystalline composite might be attributed to the synergistic effects of nanocrystalline structure, large number of grain boundaries and phase interfaces, and *in situ* formed carbon. Firstly, nanocrystalline could shorten the diffusion distance for both electron and lithium ions. Secondly, overall

conductivity of the electrode and the transportation of lithium ions can be enhanced by the *in situ* formed carbon and anatase TiO<sub>2</sub>, which result in excellent rate capability. Moreover, the higher theoretical capacities of anatase TiO<sub>2</sub> and *in situ* formed carbon could contribute partial capacity to the improved capacity of the Li<sub>4</sub>Ti<sub>5</sub>O<sub>12</sub>/TiO<sub>2</sub>/C composite. Thirdly, the abundant grain boundaries and phase interfaces in the Li<sub>4</sub>Ti<sub>5</sub>O<sub>12</sub>/TiO<sub>2</sub>/C composite can store extra lithium ions and improve the kinetics of the electrode, which make contribution to increasing the specific capacity and guaranteeing the fast lithium-ion insertion/extraction reaction.

## Conclusions

In summary, we have reported a novel strategy to synthesize Li<sub>4</sub>Ti<sub>5</sub>O<sub>12</sub>/TiO<sub>2</sub>/C nanocrystalline composite by a facile sol-gel process followed by calcination. As anode materials for LIBs, the Li<sub>4</sub>Ti<sub>5</sub>O<sub>12</sub>/TiO<sub>2</sub>/C nanocrystalline composite presents better electrochemical performance compared with pure Li<sub>4</sub>Ti<sub>5</sub>O<sub>12</sub>, Li<sub>4</sub>Ti<sub>5</sub>O<sub>12</sub>/C and Li<sub>4</sub>Ti<sub>5</sub>O<sub>12</sub>/TiO<sub>2</sub> composites, which can deliver a favorable reversible capacity of 102 mAh g<sup>-1</sup> (333 mAh cm<sup>-3</sup>) at 1 C after 100 cycles and still show a relatively high discharge capacity of 88 mAh g<sup>-1</sup> (286 mAh cm<sup>-3</sup>) at 30 C. Therefore, the Li<sub>4</sub>Ti<sub>5</sub>O<sub>12</sub>/TiO<sub>2</sub>/C nanocrystalline composite can be a potential anode material for advanced LIBs.

## Acknowledgements

This work was supported by the National Natural Science Foundation of China (51372225), and the Natural Science Foundation of Zhejiang Province, China (LY13B010001).

## Notes and references

1. J. M. Tarascon and M. Armand, *Nature*, 2001, 414, 359-367.
2. Y. Xia, Z. Xiao, X. Dou, H. Huang, X. H. Lu, R. J. Yan, Y. P. Gan, W. J. Zhu, J. P. Tu, W. K. Zhang and X. Y. Tao, *Acs Nano*, 2013, 7, 7083-7092.
3. H. Huang, W. Zhu, X. Tao, Y. Xia, Z. Yu, J. Fang, Y. Gan and W. Zhang, *Acs Appl Mater Inter*, 2012, 4, 5974-5980.
4. Y. K. Sun, S. T. Myung, B. C. Park, J. Prakash, I. Belharouak and K. Amine, *Nat Mater*, 2009, 8, 320-324.
5. M. Rahman, J. Z. Wang, M. F. Hassan, D. Wexler and H. K. Liu, *Adv Energy Mater*, 2011, 1, 212-220.
6. G. H. Jeong, H. B. Bae, D. Choi, Y. H. Kim, S. Yoon and S. W. Kim, *J Phys Chem C*, 2012, 116, 23851-23857.
7. W. Zhu, H. Yang, K. Nakanishi, K. Kanamori and X. Guo, *Rsc Adv*, 2015, 5, 24803-24813.
8. T. F. Yi, Z. K. Fang, Y. Xie, Y. R. Zhu and S. Y. Yang, *Acs Appl Mater Inter*, 2014, 6, 20205-20213.
9. J. Y. Liao, V. Chabot, M. Gu, C. M. Wang, X. C. Xiao and Z. W. Chen, *Nano Energy*, 2014, 9, 383-391.
10. W. Zhu, H. Huang, W. Zhang, X. Tao, Y. Gan, Y. Xia, H. Yang and X. Guo, *Electrochim Acta*, 2015, 152, 286-293.
11. Y. Xia, W. K. Zhang, Z. Xiao, H. Huang, H. J. Zeng, X. R. Chen, F. Chen, Y. P. Gan and X. Y. Tao,

- J Mater Chem*, 2012, 22, 9209-9215.
12. J. Wang, H. L. Zhao, Q. Yang, C. M. Wang, P. P. Lv and Q. Xia, *J Power Sources*, 2013, 222, 196-201.
13. W. J. Zhu, H. Huang, Y. P. Gan, X. Y. Tao, Y. Xia and W. K. Zhang, *Electrochim Acta*, 2014, 138, 376-382.
14. Y. M. Jiang, K. X. Wang, X. Y. Wu, H. J. Zhang, B. M. Bartlett and J. S. Chen, *Acs Appl Mater Inter*, 2014, 6, 19791-19796.
15. J. M. Sun, D. H. Teng, Y. Liu, C. Chi, Y. H. Yu, J. L. Lan and X. P. Yang, *Rsc Adv*, 2014, 4, 48632-48638.
16. J. Y. Liao, X. C. Xiao, D. Higgins, D. G. Lee, F. Hassan and Z. W. Chen, *Electrochim Acta*, 2013, 108, 104-111.
17. L. Yu, H. B. Wu and X. W. Lou, *Adv Mater*, 2013, 25, 2296-2300.
18. L. Sun, J. P. Wang, K. L. Jiang and S. S. Fan, *J Power Sources*, 2014, 248, 265-272.
19. Y. Sun, L. Zhao, H. Pan, X. Lu, L. Gu, Y.-S. Hu, H. Li, M. Armand, Y. Ikuhara and L. Chen, *Nat Commun*, 2013, 4, 1870.
20. A. Nugroho, S. J. Kim, W. Chang, K. Y. Chung and J. Kim, *J Power Sources*, 2013, 244, 164-169.
21. Y. G. Wang, H. M. Liu, K. X. Wang, H. Eiji, Y. R. Wang and H. S. Zhou, *J Mater Chem*, 2009, 19, 6789-6795.
22. H. G. Jung, N. Venugopal, B. Scrosati and Y. K. Sun, *J Power Sources*, 2013, 221, 266-271.
23. L. P. Wang, H. Q. Zhang, Q. J. Deng, Z. L. Huang, A. J. Zhou and J. Z. Li, *Electrochim Acta*, 2014, 142, 202-207.
24. X. Li, Y. Zhou, P. X. Huang, H. Peng, W. Li, M. Z. Qu, Z. L. Yu, X. B. Huang and Y. D. Chen, *Int J*

- Electrochem Sc*, 2014, 9, 4816-4825.
25. C. Lai, X. L. Cao, X. C. Yuan, Y. L. Wang and S. H. Ye, *Solid State Ionics*, 2013, 249, 151-157.
26. G. Y. Liu, H. Y. Wang, G. Q. Liu, Z. Z. Yang, B. Jin and Q. C. Jiang, *Electrochim Acta*, 2013, 87, 218-223.
27. B. T. Zhao, S. M. Jiang, C. Su, R. Cai, R. Ran, M. O. Tade and Z. P. Shao, *J Mater Chem A*, 2013, 1, 12310-12320.
28. L. Kavan, M. Kalbac, M. Zikalova, I. Exnar, V. Lorenzen, R. Nesper and M. Graetzel, *Chem Mater*, 2004, 16, 477-485.
29. Z. Q. Zhu, F. Y. Cheng and J. Chen, *J Mater Chem A*, 2013, 1, 9484-9490.
30. Y. F. Tang, F. Q. Huang, W. Zhao, Z. Q. Liu and D. Y. Wan, *J Mater Chem*, 2012, 22, 11257-11260.
31. H. C. Choi, Y. M. Jung and S. B. Kim, *Vib Spectrosc*, 2005, 37, 33-38.
32. X. Zhang, Z. Xing, L. L. Wang, Y. C. Zhu, Q. W. Li, J. W. Liang, Y. Yu, T. Huang, K. B. Tang, Y. T. Qian and X. Y. Shen, *J Mater Chem*, 2012, 22, 17864-17869.
33. Z. Song, J. Hrbek and R. Osgood, *Nano Lett*, 2005, 5, 1327-1332.
34. L. F. Shen, X. G. Zhang, E. Uchaker, C. Z. Yuan and G. Z. Cao, *Adv Energy Mater*, 2012, 2, 691-698.
35. M. Armand and J. M. Tarascon, *Nature*, 2008, 451, 652-657.
36. Y. P. Gan, L. Y. Zhu, H. P. Qin, Y. Xia, H. Xiao, L. S. Xu, L. Y. Ruan, C. Liang, X. Y. Tao, H. Huang and W. K. Zhang, *Solid State Ionics*, 2015, 269, 44-50.
37. H.-G. Jung, M. W. Jang, J. Hassoun, Y.-K. Sun and B. Scrosati, *Nat Commun*, 2011, 2, 516.
38. A. Prakash, P. Manikandan, K. Ramesha, M. Sathiya, J. Tarascon and A. Shukla, *Chem Mater*, 2010, 22, 2857-2863.

39. C. X. Peng, B. D. Chen, Y. Qin, S. H. Yang, C. Z. Li, Y. H. Zuo, S. Y. Liu and J. H. Yang, *Acs Nano*, 2012, 6, 1074-1081.
40. S. L. Xiong, J. S. Chen, X. W. Lou and H. C. Zeng, *Adv Funct Mater*, 2012, 22, 861-871.
41. L. Q. Tao, J. T. Zai, K. X. Wang, H. J. Zhang, M. Xu, J. Shen, Y. Z. Su and X. F. Qian, *J Power Sources*, 2012, 202, 230-235.
42. T. F. Yi, S. Y. Yang, M. Tao, Y. Xie, Y. R. Zhu and R. S. Zhu, *Electrochim Acta*, 2014, 134, 377-383.
43. A. Y. Shenouda and H. K. Liu, *J Alloy Compd*, 2009, 477, 498-503.
44. G. J. Du, Z. L. Liu, S. W. Tay, X. G. Liu and A. S. Yu, *Chem-Asian J*, 2014, 9, 2514-2518.
45. S.-L. Chou, J.-Z. Wang, H.-K. Liu and S.-X. Dou, *J Phys Chem C*, 2011, 115, 16220-16227.
46. J. Chen, L. Yang, S. Fang, S.-i. Hirano and K. Tachibana, *J Power Sources*, 2012, 200, 59-66.
47. L. F. Shen, E. Uchaker, X. G. Zhang and G. Z. Cao, *Adv Mater*, 2012, 24, 6502-6506.
48. Y. P. Tang, X. X. Tan, G. Y. Hou and G. Q. Zheng, *Electrochim Acta*, 2014, 117, 172-178.
49. L. Gao, R. J. Liu, H. Hu, G. J. Li and Y. Yu, *Nanotechnology*, 2014, 25.